Inorganic Chemistry
Cite This: Inorg. Chem. 2019, 58, 14403−14409
Article
pubs.acs.org/IC

Strong Solid-State Fluorescence Induced by Restriction of the Coordinate Bond Bending in Two-Coordinate Copper(I)−Carbene Complexes

Shiyun Lin,[†] Qian Peng,*[,‡] Qi Ou,[†] and Zhigang Shuai*[,†]

[†]MOE Key Laboratory of Organic OptoElectronics and Molecular Engineering, Department of Chemistry, Tsinghua University, Beijing 100084, P. R. China

[‡]CAS Key Laboratory of Organic Solids, Institute of Chemistry, Beijing National Laboratory for Molecular Sciences, Chinese Academy of Sciences, Beijing 100190, P. R. China

Supporting Information

ABSTRACT: The photophysical properties of two-coordinate copper(I) complexes have become a new research hotspot due to their nearly perfect luminescent properties and low price and promising applications in organic light-emitting diodes (OLEDs). In this work, we employ the hybrid quantum mechanics and molecular mechanics (QM/MM) approach, coupled with our early developed thermal vibration correlation function (TVCF) rate formalism, to study the aggregation effect on the luminescent properties of the cyclic (alkyl)(amino)carbene−copper(I)−Cl complex. Our calculations reveal that the transition properties changes from metal−ligand-charge-transfer (MLCT) in solution to hybrid halogen ligand charge-transfer (XLCT) and MLCT in solid state, which induces the blue-shifted emission spectra from solution to solid phase. Upon aggregation, the restriction of the bending vibrations of the C−Cu−Cl and Cu−C−N bonds largely slow down the nonradiative decay, which induces strong fluorescence. This study provides a clear rationalization for the highly efficient fluorescence character of two-coordinate Cu(I) complexes.

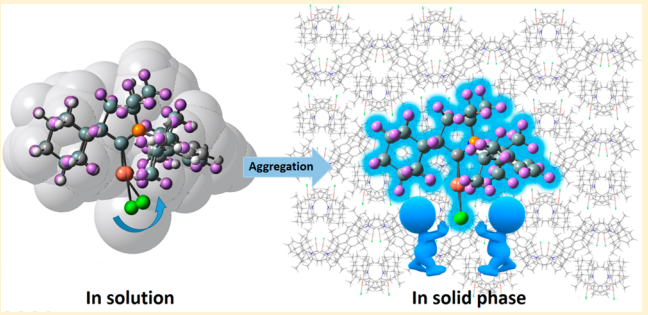

1. INTRODUCTION

The scientific investigations of the photophysical property of copper complexes have been strongly driven by the potential commercial use in OLEDs because of their outstanding advantages, such as abundance in nature, low cost, easy access, versatile coordination forms and multiple emission, etc.[1−3] Copper has two oxidation states: Cu(I) and Cu(II). The Cu(II) ion has a d^9 electronic configuration, and its complexes always produce the metal-centered (MC) state upon excitation. Since the MC state usually deactivates through ultrafast nonradiative pathways to the ground state, the luminescence for Cu(II) complexes is always very weak.[4] Different from Cu(II) complexes, Cu(I) complexes exhibit a d^{10} electronic configuration, and the filling of d orbitals prevents a d−d electronic transition to generate the MC state. Compared to other third-row heavy-metal complexes, which almost always act as triplet harvesting emitters, the copper complexes can act as both triplet and singlet harvesting emitters. This advantage is due to the weak spin−orbit coupling in copper complex and the exhibition of multiple emission such as prompt fluorescence, delayed fluorescence, and phosphorescence. These endow Cu(I) complexes with rich photophysical properties that have drawn much attention for decades.[5] Cu(I) complexes have a large variety of coordination structures, such as four-coordinate tetrahedral, three-coordinate trigonal planar, and two-coordinate linear structures, which lead to their emission spanning a wide range of the visible spectrum. Four-coordinate complexes with homoleptic $[Cu(N^{\wedge}N)_2]$ and heteroleptic $[Cu(N^{\wedge}N)(P^{\wedge}P)]$ are extensively investigated,[6−8] and many efforts have been made to reveal the mechanism of luminescence from both experiments and theoretical simulations.[9,10] Unfortunately, the four-coordinate Cu(I) complexes always suffer from a large distortion from a tetrahedral-like structure to a flattening square-planar structure during the excited-state decay because of the pseudo-Jahn−Teller (PJT) effect, which leads to a fast nonradiative deactivation. The three-coordinate Cu(I) complexes were expected not to suffer from PJT distortion. A few of three-coordinate Cu(I) complexes have been demonstrated to exhibit good luminescent performance in solid state with phosphorescence, prompt fluorescence or thermally activated delayed fluorescence (TADF).[5,11−13] However, Jahn−Teller distortion are still found to change the geometry from "Y" to "T" shaped upon excitation in the three-coordinate Cu(I) complexes.[11] The luminescent properties of two-coordinate

Received: June 9, 2019
Published: October 14, 2019

DOI: 10.1021/acs.inorgchem.9b01705
Inorg. Chem. 2019, 58, 14403−14409

Cu(I) complexes have been reported recently.[3,14−17] They exhibit highly efficient fluorescence, phosphorescence, or TADF with nearly 100% luminescence efficiency in the solid phase, which is a great breakthrough in the luminescence of copper complexes. It is necessary to reveal the mechanism of luminescence and to elucidate the property−structure relationship of the two-coordinate Cu(I) complexes. To our knowledge, little work has been done to theoretically reveal the mechanism of strong fluorescence in solid state relative to weak fluorescence in solution for the two-coordinate complexes.

In this work, we systematically and quantitatively investigate the excited-state decay dynamics for the three two-coordinate Cu(I) complexes (CAAC^{Ad})CuX (see Figure 1a) in solution

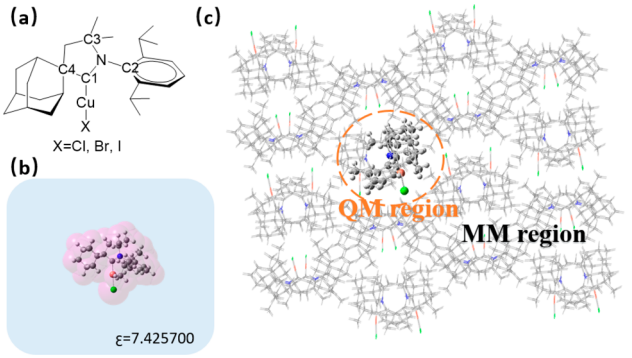

Figure 1. (a) Chemical structure of (CAAC^{Ad})CuCl. (b) Setup of PCM model. (c) Setup of QM/MM computational model.

and solid state by using PCM and hybrid quantum and molecular mechanics (QM/MM) approach and the thermal vibration correlation function (TVCF) formalism developed earlier in our group. The mechanism of their luminescence is disclosed, which should greatly benefit the molecular design of novel highly efficient two-coordinate Cu(I) complexes. From solution to aggregate, the bending vibrations of the coordinate bonds C−Cu−Cl and Cu−C−N are largely restricted, which blocks the nonradiatve decay channels and causes strong fluorescence. The deep understanding of luminescence mechanism is very helpful for the molecular design of novel highly efficient two-coordinate Cu(I) complexes.

2. COMPUTATIONAL METHODS

Based on the Fermi's golden rule (FGR), the Franck−Condon principle and the TVCF approach, the emission spectrum $\sigma_{em}(\omega,T)$ can be calculated,

$$\sigma_{em}(\omega, T) = \frac{2\omega^3}{3\pi\hbar c^3}\left|\mu_{fi}\right|^2 \int_{-\infty}^{\infty} e^{-i(\omega-\omega_{fi})t}\rho_{em}(t, T)\, dt \quad (1)$$

Here μ_{fi} is the electric transition dipole moment between two electronic states; and $\rho_{em}(t,T) = Z_i^{-1}\mathrm{Tr}(e^{i\tau_f\hat{H}_f}e^{i\tau_i\hat{H}_i})$ is TVCF which can be solved analytically by multidimensional Gaussian integrations.

The radiative decay rate constants can be calculated according to the integration over the whole emission spectrum, and gained,

$$k_r(T) = \int \sigma_{em}(\omega, T)\, d\omega \quad (2)$$

Using the FGR and first-order perturbation theory, the nonradiative internal conversion (IC) rate can be expressed as[18]

$$k_{ic} = \frac{2\pi}{\hbar}\left|H'_{fi}\right|^2\delta(E_{fi} + E_{fu} - E_{iv}) \quad (3)$$

Here the perturbation H'_{fi} is non-Born−Oppenheimer coupling, under Condon approximation which can be written as,

$$H'_{fi} = \sum_l \langle\Phi_f|\hat{P}_{fl}|\Phi_i\rangle\langle\Theta_{fu}|\hat{P}_{fl}|\Theta_{iv}\rangle \quad (4)$$

where $\hat{P}_{fl} = -i\hbar\partial/\partial Q_{fl}$ is the normal mode momentum operator.

Using the TCVF approach we can obtain

$$k_{ic} = \sum_{k,l}\frac{1}{\hbar^2}R_{kl}\int_{-\infty}^{\infty} dt\ [e^{i\omega_{if}t}\rho_{ic,kl}(t, T)] \quad (5)$$

Here $R_{kl} = \langle\Phi_f|\hat{P}_{fk}|\Phi_i\rangle\langle\Phi_i|\hat{P}_{fl}|\Phi_f\rangle$ is the nonadiabatic electronic coupling between two electronic states; and $\rho_{ic,kl}(t, T) = Z_i^{-1}\mathrm{Tr}(\hat{P}_{fk}e^{i\tau_f\hat{H}_f}\hat{P}_{fl}e^{i\tau_i\hat{H}_i})$ is the TVCF in the IC process, whose detailed solutions can be found in our previous work.[19−21]

DFT and TDDFT were employed to calculate the equilibrium geometry and the vibration frequency in the S_0 state and in the S_1 state, respectively. The LANL2DZ basis set were applied for the copper atom and 6-31G(d) for the others.[22,23] Various density functionals have been tested through comparing the optimized structure parameters in the S_0 state and spectral properties of [(CAAC^{Ad})CuCl] with the experimental counterparts (see Table S1 and Figure S1). On the basis of the test results, the M06 functional was found to be the most suitable one for the copper complex and was chosen for all the following calculations. The polarizable continuum model (PCM)[23] for tetrahydrofuran (THF) solvent was adopted in order to account for the solvent effect (see Figure 1b). The linear-response (LR) PCM was applied to the geometrical optimization and frequencies analysis, while the corrected linear-response (cLR) approach[24] was employed to obtain excitation energies accounting for the density-dependent relaxation of the solvent polarization. To account for the effect of aggregation, the ONIOM model[22] with high-level QM and low-level MM method was employed in the calculation of the geometrical and electronic structures of the cluster, which was dug from the X-ray crystal structure with size of 3 × 3 × 3 (see Figure 1c). Herein, the central molecule was treated as QM part using

Table 1. Selected Geometrical Parameters of (CAAC^{Ad})CuCl Optimized Theoretically at the S_0 and S_1 States in Solution and Solid Phase, and Obtained Experimentally from the Crystal Structure[14] (Bond Length, Ångstrom; Bond Angle, Degree)

	in solution			in solid phase			
	S_0	S_1	$\lvert\Delta(S_0 - S_1)\rvert$	S_0	S_1	$\lvert\Delta(S_0 - S_1)\rvert$	expt
Cu−C1	1.9212	1.8931	0.0281	1.9162	1.8945	0.0217	1.8830
Cu−Cl	2.1625	2.1920	0.0295	2.1336	2.1527	0.0191	2.1099
C1−N	1.3084	1.3687	0.0603	1.3111	1.3730	0.0619	1.3053
C2−N	1.4468	1.4227	0.0241	1.4492	1.4277	0.0215	1.4551
C3−N	1.5167	1.4760	0.0407	1.5150	1.4857	0.0293	1.5291
∠C1−Cu−Cl	179.50	169.83	9.67	174.45	170.79	3.66	175.33
∠Cu−C1−N	119.58	106.76	12.82	121.94	126.40	4.46	123.36
∠Cu−C1−C4	130.81	141.54	10.73	128.66	121.91	6.75	127.77

DOI: 10.1021/acs.inorgchem.9b01705
Inorg. Chem. 2019, 58, 14403−14409

(TD)M06/LANL2DZ/6-31G(d) and the surrounding molecules were treated as MM part using the universal force field (UFF). All these first-principle calculations were carried out with the *Gaussian16* program package.[24] The character of each excited-state transition was analyzed by the attachment-detachment densities[25] with Q-Chem.[26] The nonadiabatic electronic coupling term R_{kl} was treated as the force acting on the atomic nuclei through the transition electric field under the frame of the first-order perturbation theory.[27] The excited state decay rates and the spectra were calculated using the TVCF formalisms in MOMAP package.[28] The orbital composition analyses were carried out with the Multiwfn program package.[29]

3. RESULTS AND DISCUSSION

3.1. Geometric and Electronic Structures of (CAAC^{Ad})-CuCl. The main geometrical parameters of the S_0 and S_1 states of (CAAC^{Ad})CuCl in solution and solid phases are shown in Table 1, together with the X-ray crystal structure for comparison. It is obvious to see that in Table 1 the optimized geometrical parameters in the solid phase are in good agreement with the experimental crystal data. This indicates that the adopted quantum chemistry method is suitable for the complex. Analyzing the geometrical changes $|\Delta(S_0 - S_1)|$upon excitation, we can see that the complex is more flexible in solution. The largest changes appear in the coordination bond angles between copper and two ligandswith∠C1−Cu−Cl, ∠Cu−C1−N and ∠Cu−C1−C4 decreasing from 9.67°, 12.82°, and 10.73° in solution to 3.66°, 4.46°, and 6.75° in the solid phase, respectively. In addition, the bond lengths of C1−N and C3−N in the carbene ligand also change greatly in the two phases (solution, 0.0603 and 0.0407 Å; solid, 0.0619 and 0.0293 Å). These different changes in the two phases would lead to distinct photophysical properties, especially the nonradiative decay process.

The electronic structures, including main frontier molecular orbitals, their energy levels, electronic density contours, atomic components, and transition property are given in Figure 2a for

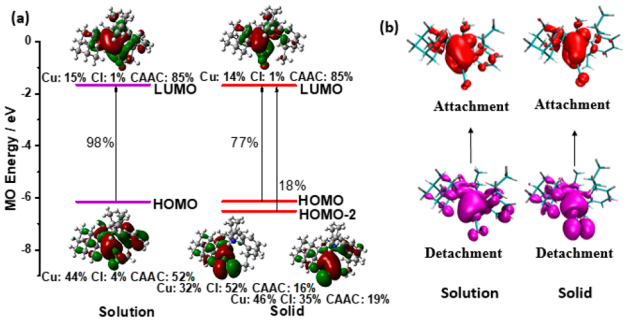

Figure 2. (a) Selected frontier molecular orbitals and the important transitions of the S_1 state at the optimized S_1 geometries in solution and solid phase. (b) Attachment-detachment densities for S_1 states at their optimized geometries in solution and solid state.

(CAAC^{Ad})CuCl at the optimized S_1 geometries in solution and the solid phase. It can be seen from Figure 2a that (i) the highest occupied molecular orbital (HOMO) is sensitive to the aggregation. It mainly localizes on copper atom (44%) and CAAC ligand (52%) in solution, while it mostly concentrates on copper atom (32%) and halogen atom (52%) in the solid phase; (ii) the lowest unoccupied orbital (LUMO) is not affected by the aggregation and is heavily confined on the CAAC ligand (85%) in both phases; (iii) the main transitions change from single HOMO → LUMO (98%) excitation in solution to double HOMO → LUMO (77%) and HOMO−2 → LUMO (18%) excitation in the solid phase. It is very clear that the transition character changes from metal-to-ligand charge transfer (MLCT) to hybrid MLCT and halogen-to-ligand charge transfer (XLCT) upon aggregation. Consequently, the excitation energy increases from 2.88 to 2.95 eV due to the participation of the deeper orbitals in the solid state, which is confirmed by the blue shift of the emission spectrum relative to that in solution observed in experiment.[14] The attachment−detachment densities (which are more intuitive than MOs) are shown in Figure 2b at the optimized S_1 geometries in solution and the solid phase for (CAAC^{Ad})CuCl. From Figure 2b, it is obvious that the electron transitions can be assigned to MLCT in solution, and mixing MLCT/XLCT in solid phase.

3.2. Photophysical Properties of (CAAC^{Ad})CuCl. The vibrationally resolved absorption and emission spectra are calculated for (CAAC^{Ad})CuCl at 298 K in solution and solid phase, and plotted in Figure 3 together with the available

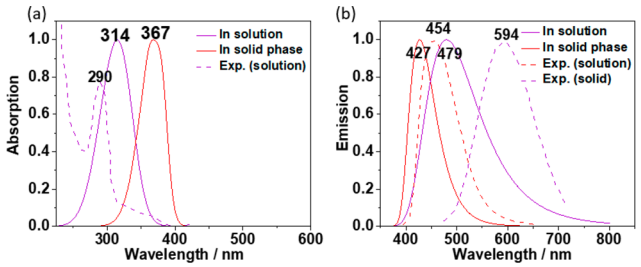

Figure 3. Calculated (a) absorption and (b) emission spectra of (CAAC^{Ad})CuCl in solution and solid phase with experiment data.

experimental emission spectrum for comparison. Compared with the optical spectra in solution, the emission spectrum in aggregate shows a large blue shift which agrees well with the experimental observation,[14] while the absorption spectrum exhibit an obvious red shift. As a result, the Stokes shift is greatly reduced from solution to solid phase. The adiabatic excitation energy changes slightly from 3.33 eV in solution to 3.26 eV in solid phase. Such changes of optical spectra suggest that the reorganization energy would be sharply decreased and the nonradiative decay channels would be greatly restricted correspondingly in solid phase.[30] The vibrationally resolved spectra at low temperature can be used to elucidate the electronic transition properties and electron−phonon interaction. Therefore, the individual emission peaks are assigned to the involved vibrational states as shown in Figure S5. The maximum emission peaks come from the vibration of 126.72 cm^{-1}, which can be related to the C−Cu−Cl bending. The bending vibration can be related to blue shift in the simulated emission spectra.

The calculated radiative and nonradiative decay rate constants of (CAAC^{Ad})CuCl in solution and solid phase are given in Table 2, as well as the oscillator strength and vertical excitation energy based on the geometries of S_1 states. From Table 2, it can be seen that from solution to solid phase both oscillator strength and adiabatic excitation energy change a little. Thus, the radiative decay rate constants are close in both phases. Differently, upon aggregation the internal conversion rate constant k_{ic} decreases by about 4 orders of magnitude. In addition, the intersystem crossing rate constants are very small of ca. 10^2 s^{-1} in both phases. The resultant fluorescence

DOI: 10.1021/acs.inorgchem.9b01705
Inorg. Chem. 2019, 58, 14403−14409

Table 2. Calculated Oscillator Strength, Vertical Excitation Energy, Radiative, Non-Radiative, and Intersystem Crossing Decay Rate Constants, and Fluorescence Quantum Yield of (CAAC^{Ad})CuCl in Solution and Solid Phase at 298 K (A, in Solution; B, in the Solid Phase)

	f	ΔE/eV	k_r/s^{-1}	k_{ic}/s^{-1}	k_{isc}/s^{-1}	Φ_F/%
A	0.0030	2.87	6.26×10^5	8.38×10^7	9.18×10^2	0.44
B	0.0024	2.95	7.83×10^5	1.47×10^4	1.21×10^2	98.0

quantum yield (Φ_F) increases from 0.44% to 98% upon aggregation, which is very close to the experiment value of 96% in solid state.[14]

3.3. The Mechanism of Luminescence of (CAAC^{Ad})-CuCl. As discussed above, the remarkable decrease of the internal conversion rate constant induced strong emission in solid state. In order to deeply understand the intrinsic mechanism, we revisit the formalism of the k_{ic} and extract two important factors to manipulate the rate constant. One is the nonadiabatic coupling, which provides a driving force to the excited-state decay. In the conventional linear coupling model of nonradiative rate theory, the normal modes with the largest nonadiabatic coupling matrix element are defined as "promoting mode.[31] The other factor is the reorganization energy which characterizes the ability of normal modes to accept excess excited-state energy.[20,32] The normal modes with largest reorganization energy are as called "accepting mode".[31] In the multimode coupling model of the nonradiative rate theory in MOMAP program, the concept of "promoting/accepting mode" has been abandoned, and any normal modes can act as "promoting mode" or "accepting mode". In other words, all the modes are considered through diagonal and nondiagonal elements of the nonadiabatic coupling matrix.[18]

For a more intuitive analysis of the change in nonadiabatic couplings upon aggregation, we only plotted the diagonal parts in Figure 4. It is seen that the couplings become much smaller

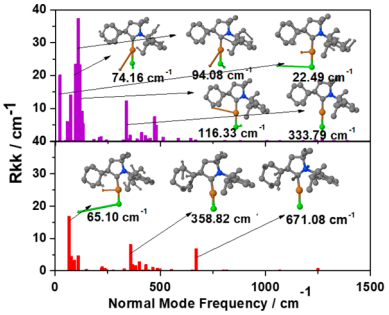

Figure 4. Diagonal elements of the electronic coupling matrix versus the normal mode index of (CAAC^{Ad})CuCl in solution and solid phases.

from solution to solid phase. In solution, the low frequency vibrations of 22.49, 74.16, 97.08, and 116.33 cm^{-1} have large nonadiabatic couplings, and these modes belong to the bending vibrations of bond C−Cu−Cl. The stretching vibration of bond Cu−Cl of 337.79 cm^{-1} also makes a relatively high contribution in nonadiabatic couplings. In contrast, this kind of vibrations are hugely suppressed in solid phase; only the modes of 65.10 cm^{-1} makes a contribution. In addition, the stretching mode of C−N appears in high-frequency region. Overall, the nonadiabatic couplings are highly suppressed in solid phase, which can lead to a large decrease in nonradiative decay rate.

The reorganization energies were calculated by the formula $\lambda_l = \omega_l^2 D_l^2/2$, D_l is the displacement along the lth normal mode between two electronic states. Results are shown in Figure 5a,

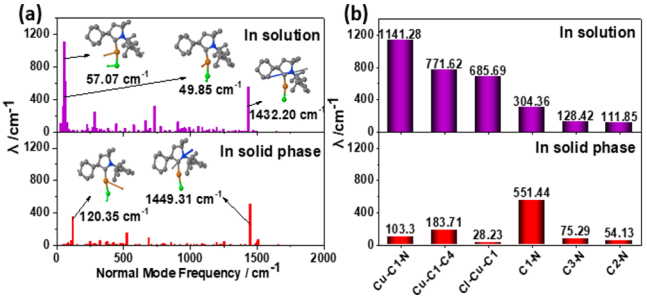

Figure 5. (a) Reorganization energy (λ) based on the potential surface in the S_1 state for (CAAC^{Ad})CuCl, as well as their contributed vibration modes; (b) projection of the reorganization energies onto the internal coordinates in solution and solid phases.

as well as the displacement vectors of important modes for (CAAC^{Ad})CuCl in solution and solid phases. The total reorganization energies decrease a lot from solution (7121 cm^{-1}) to solid state (2274 cm^{-1}). From Figure 5a, we can visually find that the largest contributions to the reorganization energy come from several low-frequency modes and one high-frequency mode in solution. Their frequencies/reorganization energies are 49.85 cm^{-1}/309.18 cm^{-1}, 57.07 cm^{-1}/1120.00 cm^{-1}, 65.51 cm^{-1}/630.01 cm^{-1}, and 1432.20 cm^{-1}/555.61 cm^{-1}, respectively. In comparison, there are only one low-frequency mode (ω = 120.35 cm^{-1}, λ = 347.75 cm^{-1}) and one high-frequency mode (ω = 1449.31 cm^{-1}, λ = 508.79 cm^{-1}) in the solid phase. From the displacement vectors in Figure 5a, these low-frequency modes are assigned to be the bending vibrations associated with coordination bonds C1−Cu and Cu−Cl, and the high-frequency mode belongs to the stretching vibration of C−N bond in carbene ligand. These features are in good agreement with the geometrical modifications discussed above. Upon aggregation, the vibrations of angles C1−Cu−Cl and Cu−C1−N are restricted largely, while the stretching vibrations of C1−N bond is insensitive to the environment. The same features can be found from the reorganization energies at the S_0 state given in Figure S3 and the Huang−Rhys factor versus the normal modes frequencies shown in Figure S4. The change of the reorganization energy again leads to a great decrease of the nonradiative decay rate upon aggregation.

In order to establish the structure−property relationship, we further project the reorganization energies onto the internal coordinates. The important bond lengths, bond angles and dihedral angles with large reorganization energy are plotted in Figure 5b for (CAAC^{Ad})CuCl in both solution and solid phase. It is obvious that the bond angles Cu−C1−N, C1−Cu−Cl, and Cu−C1−C4 are the most sensitive parameters to the environment. For example, the reorganization energy of the bond angle Cu−C1−N is highly suppressed from 1141.28 to

DOI: 10.1021/acs.inorgchem.9b01705
Inorg. Chem. 2019, 58, 14403−14409

103.3 cm^{-1}. The reorganization energy of bond angle Cu−C1−C4 greatly decreases from 771.62 to 183.71 cm^{-1}. The bond angle C1−Cu−Cl makes large contribution to the reorganization energy of 685.69 cm^{-1} in solution, while its contribution vanishes in solid phase. The impacts of the bond lengths C1−N, C2−N, C3−N abate to some extent upon aggregation.

Overall, the strong solid-state fluorescence is induced by the restriction of the bending vibrations of coordination bonds for the complex ($CAAC^{Ad}$)CuCl. This is quite different from the traditional aggregation induced emission (AIE)[33] caused by the restriction of rotational,[34] twisting[35] and stretching[36] vibrations.

3.4. Similar Luminescence Mechanism in ($CAAC^{Ad}$)-CuBr and ($CAAC^{Ad}$)CuI. In order to confirm the universality of the luminescence mechanism for the two-coordinate Cu(I) complexes with similar chemical structure, we explore the photophysical properties of ($CAAC^{Ad}$)CuBr and ($CAAC^{Ad}$)-CuI. As expected, similar results are found in both complexes: they both present large improvements of fluorescence luminescence for the decrease of nonradiative decay rates from solution to solid phase (the radiative and nonradiative rate constants are shown in Table S5). The change of nonradiative decay can be attributed to the decrease of reorganization energy as Figure 6 shown. Herein, the low

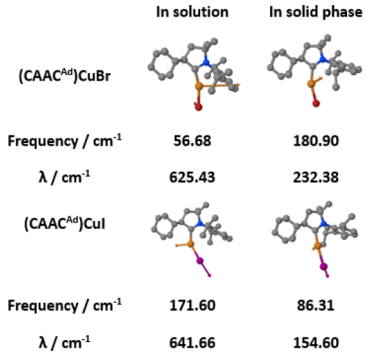

Figure 6. Selected vibrations with reorganization energy (λ) of ($CAAC^{Ad}$)CuBr and ($CAAC^{Ad}$)CuI in solution and solid phase.

frequency bending vibrations are much restricted from solution to solid phase similarly. (the other important vibrations and their reorganization energy are also listed in Table S6 and S7). What's more, their absorption and emission spectrum are shown in Figure S6 and S7. Red-shifts in absorption and blue-shift in emission from solution to solid phase are also observed, which is the same as copper chloride complex.

4. CONCLUSIONS

In summary, the luminescent properties of two-coordinate Cu(I)−carbene complexes were investigated in solution and solid phase by using PCM and QM/MM approaches coupled with the TVCF formalism. Through comprehensive analysis of the geometrical and electronic structures, reorganization energy, nonadiabatic coupling, absorption and emission spectra, and the radiative and nonradiative decay rates in the two phases, we conclude that (i) the calculated geometry, spectral behavior, and fluorescence quantum efficiency are in good agreement with the available experimental data; (ii) from solution to solid phase, the nature of the electronic excitation changes from MLCT to hybrid MLCT/XLCT; (iii) the bending motions of the bond angles C−Cu−Cl and Cu−C−N are greatly restricted from solution to solid phase, which is manifested in the changes of geometrical structures, reorganization energy, and nonadiabatic coupling; (iv) at ambient temperature, the nonradiative decay rate is decreased by about 3−4 orders of magnitude upon aggregation, and the solid-state Φ_F increases to 98% from 0.44% in solution. The restriction of the bending vibrations of bond angles C−Cu−Cl and Cu−C−N induced the strong solid-state fluorescence, which is quite different from the existing AIE systems induced by the restriction of rotational and twisting vibrations. These indicate that the surrounding environments of bond angles C−Cu−Cl and Cu−C−N should be paid close attention, in order to recover the strong fluorescence via either single molecular design or modulation of aggregation for the two-coordinate Cu(I) complexes. Moreover, the same mechanism is found in the two-coordinate copper(I) complexes with similar chemical structure. The deep understanding of the luminescence mechanism at microscopic level would be helpful for designing novel highly efficient solid-state luminescent copper complex materials. Here, we only investigated the fluorescence properties for the two-coordinate Cu(I) complexes, and we will explore the TADF and phosphorescence mechanisms of two-coordinate Cu(I) complexes in our future work.

■ ASSOCIATED CONTENT

Supporting Information

The Supporting Information is available free of charge on the ACS Publications website at DOI: 10.1021/acs.inorgchem.9b01705.

Calculated reorganization energy, Huang−Rhys factor, and photophyiscal properties for Cu(I) complexes in different phases, as well as their contributed vibration modes (PDF)

■ AUTHOR INFORMATION

Corresponding Authors

*E-mail: qpeng@iccas.ac.cn (Q.P.).
*E-mail: zgshuai@tsinghua.edu.cn (Z.S.).

ORCID

Qian Peng: 0000-0001-8975-8413
Zhigang Shuai: 0000-0003-3867-2331

Notes

The authors declare no competing financial interest.

■ ACKNOWLEDGMENTS

This work is supported by the National Natural Science Foundation of China (Grant No. 21788102), the Ministry of Science and Technology of China (Grant Nos. 2017YFA0204501 and 2015CB65502), and the Strategic Priority Research Program of the Chinese Academy of Sciences (Grant No. XDB12020200).

■ REFERENCES

(1) Dumur, F. Recent advances in organic light-emitting devices comprising copper complexes: A realistic approach for low-cost and highly emissive devices? *Org. Electron.* **2015**, *21*, 27−39.
(2) Yersin, H. *Highly efficient OLEDs: Materials based on thermally activated delayed fluorescence*; Wiley-VCH: 2018.
(3) Di, D.; Romanov, A. S.; Yang, L.; Richter, J. M.; Rivett, J. P. H.; Jones, S.; Thomas, T. H.; Abdi Jalebi, M.; Friend, R. H.; Linnolahti, M.; Bochmann, M.; Credgington, D. High-performance light-emitting

DOI: 10.1021/acs.inorgchem.9b01705
Inorg. Chem. 2019, 58, 14403−14409

diodes based on carbene-metal-amides. *Science* **2017**, *356* (6334), 159−163.
(4) Zhang, X.; Jacquemin, D.; Peng, Q.; Shuai, Z.; Escudero, D. General Approach To Compute Phosphorescent OLED Efficiency. *J. Phys. Chem. C* **2018**, *122* (11), 6340−6347.
(5) Czerwieniec, R.; Leitl, M. J.; Homeier, H. H. H.; Yersin, H. Cu(I) complexes - Thermally activated delayed fluorescence. Photophysical approach and material design. *Coord. Chem. Rev.* **2016**, *325*, 2−28.
(6) Chen, J.-L.; Zeng, X.-H.; Luo, Y.-S.; Wang, W.-M.; He, L.-H.; Liu, S.-J.; Wen, H.-R.; Huang, S.; Liu, L.; Wong, W.-Y. Synthesis, structure, and photophysics of copper(i) triphenylphosphine complexes with functionalized 3-(2′-pyrimidinyl)-1,2,4-triazole ligands. *Dalton Trans* **2017**, *46* (38), 13077−13087.
(7) He, L.-H.; Luo, Y.-S.; Di, B.-S.; Chen, J.-L.; Ho, C.-L.; Wen, H.-R.; Liu, S.-J.; Wang, J.-Y.; Wong, W.-Y. Luminescent Three- and Four-Coordinate Dinuclear Copper(I) Complexes Triply Bridged by Bis(diphenylphosphino)methane and Functionalized 3-(2′-Pyridyl)-1,2,4-triazole Ligands. *Inorg. Chem.* **2017**, *56* (17), 10311−10324.
(8) Liu, L.-P.; Li, Q.; Xiang, S.-P.; Liu, L.; Zhong, X.-X.; Liang, C.; Li, G. H.; Hayat, T.; Alharbi, N. S.; Li, F.-B.; Zhu, N.-Y.; Wong, W.-Y.; Qin, H.-M.; Wang, L. Near-saturated red emitters: four-coordinate copper(i) halide complexes containing 8-(diphenylphosphino)-quinoline and 1-(diphenylphosphino)naphthalene ligands. *Dalton Trans* **2018**, *47* (28), 9294−9302.
(9) Mara, M. W.; Fransted, K. A.; Chen, L. X. Interplays of excited state structures and dynamics in copper(I) diimine complexes: Implications and perspectives. *Coord. Chem. Rev.* **2015**, *282*−*283*, 2−18.
(10) Iwamura, M.; Takeuchi, S.; Tahara, T. Ultrafast Excited-State Dynamics of Copper(I) Complexes. *Acc. Chem. Res.* **2015**, *48* (3), 782−791.
(11) Hashimoto, M.; Igawa, S.; Yashima, M.; Kawata, I.; Hoshino, M.; Osawa, M. Highly Efficient Green Organic Light-Emitting Diodes Containing Luminescent Three-Coordinate Copper(I) Complexes. *J. Am. Chem. Soc.* **2011**, *133* (27), 10348−10351.
(12) Krylova, V. A.; Djurovich, P. I.; Conley, B. L.; Haiges, R.; Whited, M. T.; Williams, T. J.; Thompson, M. E. Control of emission colour with N-heterocyclic carbene (NHC) ligands in phosphorescent three-coordinate Cu(i) complexes. *Chem. Commun.* **2014**, *50* (54), 7176−7179.
(13) Leitl, M. J.; Krylova, V. A.; Djurovich, P. I.; Thompson, M. E.; Yersin, H. Phosphorescence versus Thermally Activated Delayed Fluorescence. Controlling Singlet-Triplet Splitting in Brightly Emitting and Sublimable Cu(I) Compounds. *J. Am. Chem. Soc.* **2014**, *136* (45), 16032−16038.
(14) Romanov, A. S.; Di, D.; Yang, L.; Fernandez-Cestau, J.; Becker, C. R.; James, C. E.; Zhu, B.; Linnolahti, M.; Credgington, D.; Bochmann, M. Highly photoluminescent copper carbene complexes based on prompt rather than delayed fluorescence. *Chem. Commun.* **2016**, *52* (38), 6379−6382.
(15) Gernert, M.; Müller, U.; Haehnel, M.; Pflaum, J.; Steffen, A. A Cyclic Alkyl(amino)carbene as Two-Atom π-Chromophore Leading to the First Phosphorescent Linear CuI Complexes. *Chem. - Eur. J.* **2017**, *23* (9), 2206−2216.
(16) Hamze, R.; Peltier, J. L.; Sylvinson, D.; Jung, M.; Cardenas, J.; Haiges, R.; Soleilhavoup, M.; Jazzar, R.; Djurovich, P. I.; Bertrand, G.; Thompson, M. E. Eliminating nonradiative decay in Cu(I) emitters: > 99% quantum efficiency and microsecond lifetime. *Science* **2019**, *363* (6427), 601−606.
(17) Taffet, E. J.; Olivier, Y.; Lam, F.; Beljonne, D.; Scholes, G. D. Carbene-Metal-Amide Bond Deformation, Rather Than Ligand Rotation, Drives Delayed Fluorescence. *J. Phys. Chem. Lett.* **2018**, *9* (7), 1620.
(18) Niu, Y.; Peng, Q.; Shuai, Z. Promoting-mode free formalism for excited state radiationless decay process with Duschinsky rotation effect. *Sci. China, Ser. B: Chem.* **2008**, *51* (12), 1153−1158.
(19) Peng, Q.; Niu, Y.; Shi, Q.; Gao, X.; Shuai, Z. Correlation function formalism for triplet excited state decay: combined spin-orbit and nonadiabatic couplings. *J. Chem. Theory Comput.* **2013**, *9* (2), 1132−1143.
(20) Shuai, Z.; Peng, Q. Organic Light-emitting Diodes: Theoretical Understanding of Highly Efficient Materials and Development of Computational Methodology. *Natl. Sci. Rev.* **2017**, *4* (2), 224−239.
(21) Peng, Q.; Yi, Y.; Shuai, Z.; Shao, J. Excited state radiationless decay process with Duschinsky rotation effect: Formalism and implementation. *J. Chem. Phys.* **2007**, *126* (11), 114302.
(22) Maseras, F.; Morokuma, K. IMOMM: A new integrated ab initio + molecular mechanics geometry optimization scheme of equilibrium structures and transition states. *J. Comput. Chem.* **1995**, *16* (9), 1170.
(23) Caricato, M.; Mennucci, B.; Tomasi, J.; Ingrosso, F.; Cammi, R.; Corni, S.; Scalmani, G. Formation and relaxation of excited states in solution: A new time dependent polarizable continuum model based on time dependent density functional theory. *J. Chem. Phys.* **2006**, *124* (12), 124520.
(24) Frisch, M.; Trucks, G.; Schlegel, H.; Scuseria, G.; Robb, M.; Cheeseman, J.; Scalmani, G.; Barone, V.; Petersson, G.; Nakatsuji, H.; *Gaussian 16*, revision A. 03; Gaussian Inc.: Wallingford, CT, 2016.
(25) Head-Gordon, M.; Grana, A. M.; Maurice, D.; White, C. A. Analysis of Electronic Transitions as the Difference of Electron Attachment and Detachment Densities. *J. Phys. Chem.* **1995**, *99* (39), 14261−14270.
(26) Kong, J.; White, C. A.; Krylov, A. I.; Sherrill, D.; Adamson, R. D.; Furlani, T. R.; Lee, M. S.; Lee, A. M.; Gwaltney, S. R.; Adams, T. R.; Ochsenfeld, C.; Gilbert, A. T. B.; Kedziora, G. S.; Rassolov, V. A.; Maurice, D. R.; Nair, N.; Shao, Y.; Besley, N. A.; Maslen, P. E.; Dombroski, J. P.; Daschel, H.; Zhang, W.; Korambath, P. P.; Baker, J.; Byrd, E. F. C.; Van Voorhis, T.; Oumi, M.; Hirata, S.; Hsu, C.-P.; Ishikawa, N.; Florian, J.; Warshel, A.; Johnson, B. G.; Gill, P. M. W.; Head-Gordon, M.; Pople, J. A. Q-Chem 2.0: a high-performance ab initio electronic structure program package. *J. Comput. Chem.* **2000**, *21* (16), 1532−1548.
(27) Lin, S. H. Rate of Interconversion of Electronic and Vibrational Energy. *J. Chem. Phys.* **1966**, *44* (10), 3759−3767.
(28) Niu, Y.; Li, W.; Peng, Q.; Geng, H.; Yi, Y.; Wang, L.; Nan, G.; Wang, D.; Shuai, Z. MOlecular MAterials Property Prediction Package (MOMAP) 1.0: a software package for predicting the luminescent properties and mobility of organic functional materials. *Mol. Phys.* **2018**, *116*, 1078−1090.
(29) Lu, T.; Chen, F. Multiwfn: a multifunctional wavefunction analyzer. *J. Comput. Chem.* **2012**, *33* (5), 580.
(30) Wu, Q.; Zhang, T.; Peng, Q.; Wang, D.; Shuai, Z. Aggregation induced blue-shifted emission - the molecular picture from a QM/MM study. *Phys. Chem. Chem. Phys.* **2014**, *16* (12), 5545−5552.
(31) Lin, S.; Chang, C.; Liang, K.; Chang, R.; Zhang, J.; Yang, T.; Hayashi, M.; Shiu, Y.; Hsu, F. Ultrafast dynamics and spectroscopy of bacterial photosynthetic reaction centers. *Adv. Chem. Phys.* **2002**, *121*, 1−88.
(32) Reimers, J. R. A practical method for the use of curvilinear coordinates in calculations of normal-mode-projected displacements and Duschinsky rotation matrices for large molecules. *J. Chem. Phys.* **2001**, *115* (20), 9103−9109.
(33) Tang, B. Z.; Zhan, X.; Yu, G.; Sze Lee, P. P.; Liu, Y.; Zhu, D. Efficient blue emission from siloles. *J. Mater. Chem.* **2001**, *11* (12), 2974−2978.
(34) Zhang, T.; Peng, Q.; Quan, C.; Nie, H.; Niu, Y.; Xie, Y.; Zhao, Z.; Tang, B. Z.; Shuai, Z. Using the isotope effect to probe an aggregation induced emission mechanism: theoretical prediction and experimental validation. *Chemical science* **2016**, *7* (8), 5573−5580.
(35) Bu, F.; Duan, R.; Xie, Y.; Yi, Y.; Peng, Q.; Hu, R.; Qin, A.; Zhao, Z.; Tang, B. Z. Unusual Aggregation-Induced Emission of a Coumarin Derivative as a Result of the Restriction of an Intramolecular Twisting Motion. *Angew. Chem., Int. Ed.* **2015**, *54* (48), 14492−14497.
(36) Ma, H.; Shi, W.; Ren, J.; Li, W.; Peng, Q.; Shuai, Z. Electrostatic interaction-induced room-temperature phosphorescence

DOI: 10.1021/acs.inorgchem.9b01705
Inorg. Chem. 2019, 58, 14403−14409

in pure organic molecules from QM/MM calculations. *J. Phys. Chem. Lett.* **2016**, *7* (15), 2893−2898.

DOI: 10.1021/acs.inorgchem.9b01705
Inorg. Chem. 2019, 58, 14403−14409